Effects of ethylenediamine on the intrinsic photoresponse of PbS quantum dots

Patrick Michel, Mario Martin , Jonas Hiller and Marcus Scheele

1. ASOPS operating details

As discussed in the main manuscript, we employ Asynchronous Optical Sampling (ASOPS), a two-pulse correlation technique that enables ultrafast time-resolved measurements on the nanosecond timescale, with a temporal resolution reaching down to few tens of femtoseconds, limited only by the pulse width of >90 fs. For this purpose, we utilize an Optical Sampling Engine (OSE) developed by Menlo Systems, which generates the two laser pulses necessary for ASOPS, at a wavelength of 1560 (±20) nm. These are emitted with a repetition frequency (f_{rep}) 100 MHz (Laser A) and 100 MHz ± Δf (Laser B), respectively. A schematic illustration of the ASOPS operating principle is provided in **Figure S1**.

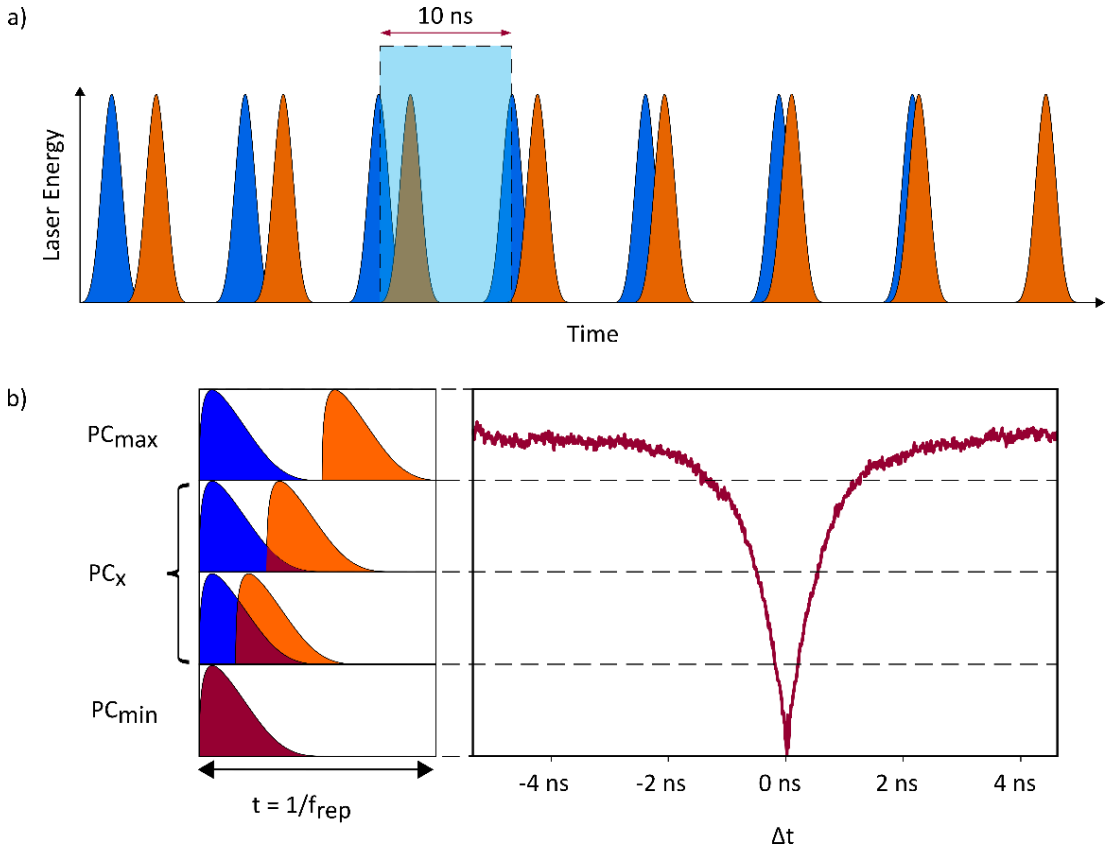

Figure S1: a) Schematic depiction of the Optical Sampling Engine (OSE) of the ASOPS system. On the leftmost side we observe the two separated lasers, laser A (100 MHz, blue) and laser B (100 MHz - Δf, orange). As time increases the pulses become increasingly closer, by the difference in frequency (Δf). In **b)** we can observe the resulting photocurrent resulting from the

pulse distance of the lasers. As the separation between the pulses decreases, the system is re-exited before a relaxation and the resulting change in measured photocurrent leads to the spectra shown on the right side of **b).**

The beat frequency (Δf), and therefore the delay time between the lasers, is of especial importance as it defines the resolution limit for the performed measurements. As per operating specifications it can vary from 10 kHz down to 1 Hz which corresponds to a temporal resolution of 1 ps and 0.1 fs, respectively. This is determined by $t_{res} = \Delta f/(f_{rep} \cdot (f_{rep} + \Delta f)) \sim \Delta f/f_{rep}^2$. In our measurements, we usually measure at a beat frequency of 100 Hz, which would enable a maximum resolution of 10 fs. Since the pulses of the system have a width of >90 fs, we are therefore measuring at the resolution limit of our system. Data acquisition is performed at a 600 MHz Ultra high frequency Lock-in Amplifier (UHFLI) by Zurich instruments, which locks onto an input frequency to get a significantly better signal to noise ratio.

The input frequency for our system is the beat frequency, which means that data acquisition is not done at each new pulse of the actual laser system (operating at 100 MHz) but each datapoint is acquired at a 1 ms interval, which is well within the specifications of the lock-in amplifier and bypasses the actual detection limit. The beat frequency is however not exactly defined, but it slightly varies, and its exact number is relayed from the OSE, (where it is calibrated through a complex system of feedback loops) to the UHFLI to avoid overlap with different relative pulse positions. Before data acquisition, the signal is amplified using a transimpedance amplifier, usually operating at a magnification factor of 10^4.

The intrinsic response time, t_r , of the system is determined by the following relation[1]:

$$\frac{1}{t_r} = \frac{1}{t_{rec}} + \frac{1}{t_{transit}}$$

where t_{rec} denotes the carrier recombination-, and $t_{transit}$ represents the carrier transit-time. The transit time can be further expressed as:

$$t_{transit} = \frac{l^2}{\Delta V}$$

with l corresponding to the channel length and ΔV to the applied bias voltage across the system. In many scenarios however, the contribution of the transit time is negligible in relation to the total response time, which is predominantly governed by the recombination time. To evaluate the contribution of the transit time in our system, we examine the applied bias, with the resulting spectra presented in the **Figure S2**.

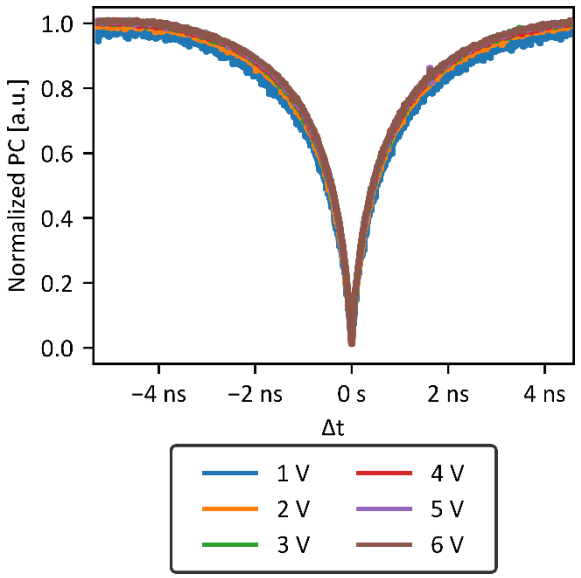

Figure S2: Intrinsic response time of a PbS/EDA QD film under vacuum at different applied bias voltages.

In this figure, we observe that the applied bias voltage, and therefore the transit time, does not impact our system to an extent in which it would require more explicit consideration. Nonetheless, we consistently perform our ASOPS measurements with interdigitate electrodes of 2.5 µm channel length and bias voltages of typically 5 V or 3 V.

The lower bias voltage was mainly used to get a signal when external signals were detected, leading to an overload of the UHFLI. The impact of external frequencies on our signal is elaborated on in **Section 3**.

2. SEM Images and morphology overview

We attempt to provide a more detailed analysis of the influence of ligands on the morphology of the resulting films. However, accurately characterizing the morphological differences between the different films presents several challenges. Firstly, the films are not homogeneous, and they cover the entire substrate. As a result, the scanning electron microscope (SEM) images in **Figure S3** represent only a small fraction of the total film area, even when only observing the film between the used electrodes, making it difficult to analyse the entire substrate for an accurate representation of the film structure. While our observation that film morphology exhibits slight variations depending on the ligand used is generally valid, the indicated trend lacks sufficient consistency to state a direct correlation between the observed morphology and the variations observed in our photocurrent measurements. Additional films prepared using a standard spin-coating protocol (described in the experimental section of the main text) display further indications for the stated morphological differences (**Figure S3**).

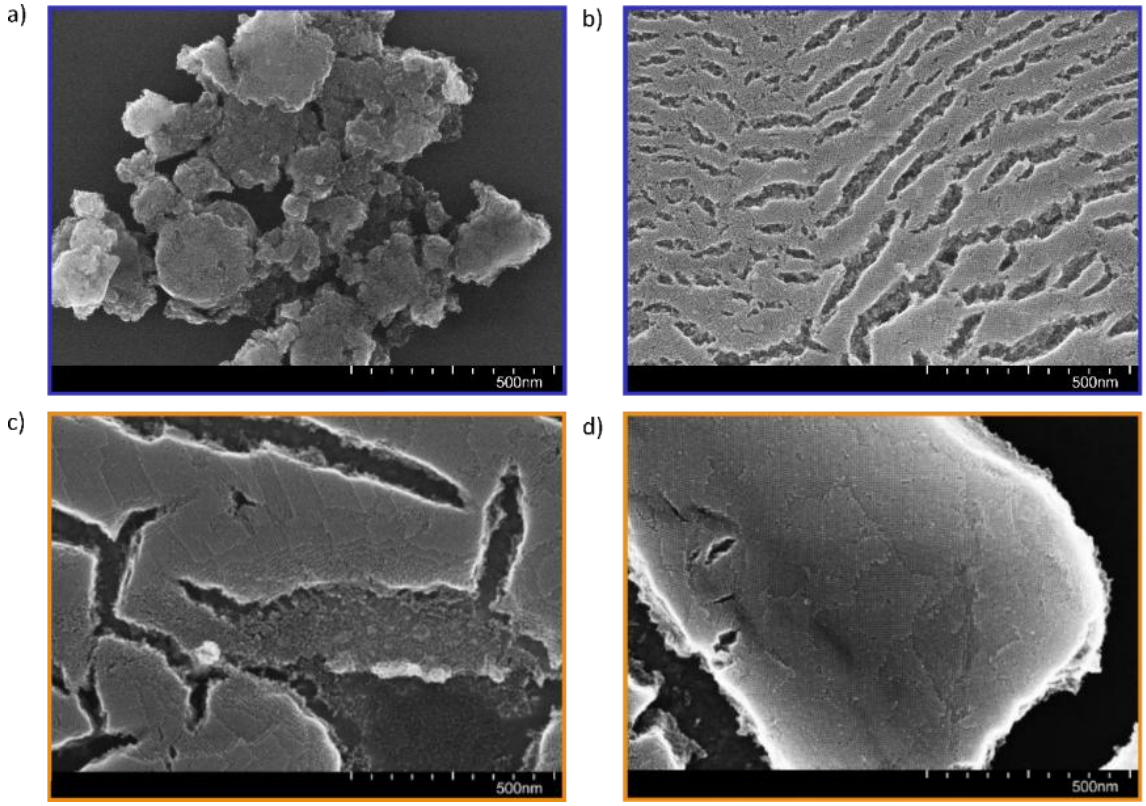

Figure S3: a,c) Measurements of two different samples of PbS/EDT QDs. **b,d)** Measurements of two different samples of PbS/EDA QDs. The blue/orange marker indicated that the experiments were performed on the same day with the same preparation conditions.

Nanoparticle aggregation, which leads to film cracking, is evident in films prepared with both ligands, as shown in **Figure S4**. A lower magnification was selected to better illustrate the morphological differences between the two films. In the case of PbS/EDT, aggregation is consistently observed across the sample. In contrast, the film of PbS/EDA exhibits similar aggregation behaviour, but it is less uniformly pronounced, with portions of the film appearing largely unaffected by the ligand exchange process.

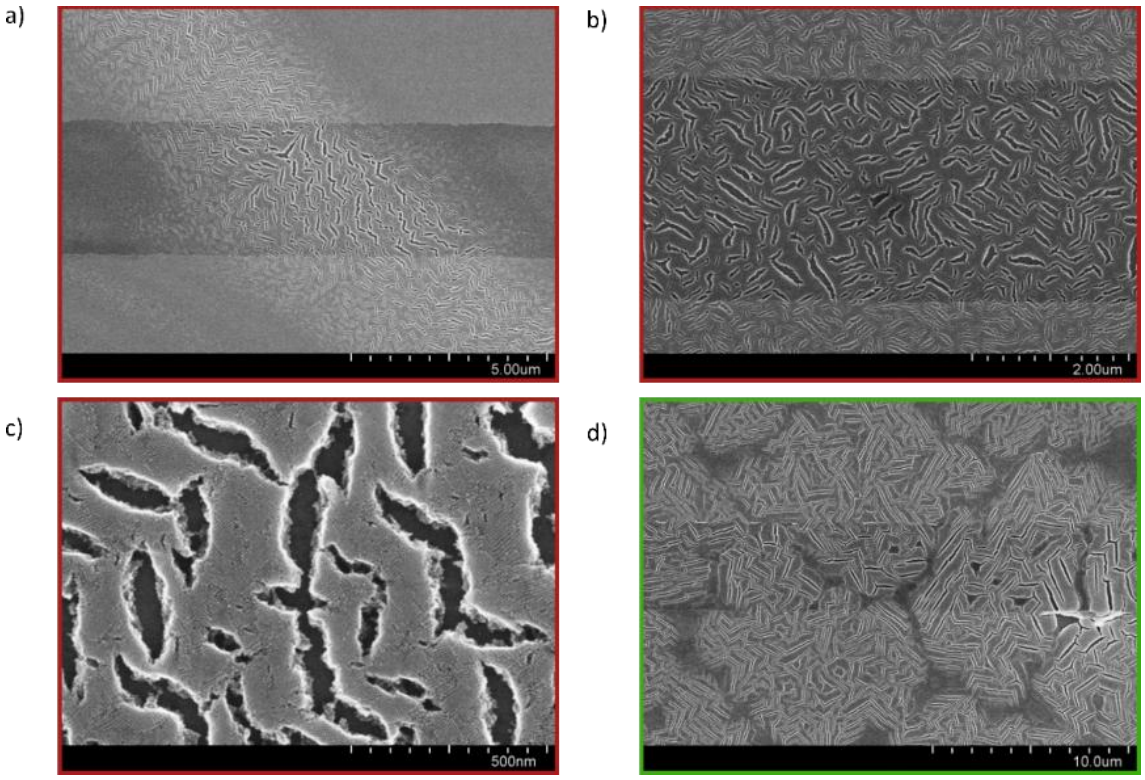

Figure S4: a,b,c) Measurements of PbS/EDA QDs at different magnifications **d)** Measurement of PbS/EDT. Both samples were prepared via drop casting.

3. Additional ASOPS measurements and signal verification

3.1. Influences of external signals and Instruments

Although all measurements were performed in a Faraday cage-like probe station (LakeShore Cryotronics CRX-6.5K), they initially appeared to be susceptible to modulation from various external sources. These included the frequency of the pump associated with the cryostat used for temperature-dependent measurements, as well as interference from well as other equipment not directly related to the photocurrent experiment. The influences lead to a lack of symmetry at Δt = 0 s. This is evident in **Figure S5 a)**, where frequency modulation affects the signal differently at various acquisition times, and even more so in **Figure S5 b)**, where measurements taken only seconds apart (while the cryostat was active) show significant differences.

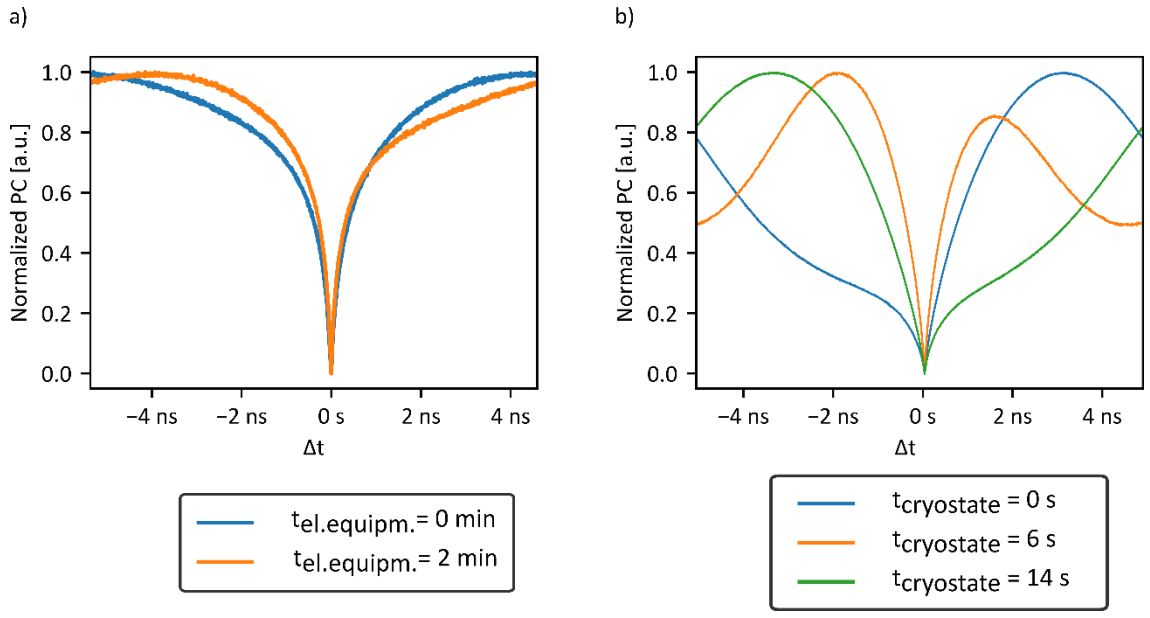

Figure S5: a) AOSPS data of PbS/EDA-exchanged nanoparticles acquired in the presence of various nearby measurement instruments, recorded at two different time points. **b)** AOSPS data of the same sample with the cryostat actively operating. All measurements from a) and b) were recorded at a delay frequency of Δf = –100 Hz. $t_{el.equipment}$ and $t_{cryostate}$ indicate the time at which the signal was recorded. In case of b) this means that the measurement shown in blue was recorded at t=0, and the orange measurements 6 seconds after (t =6s). Each measurement was recorded with >1s per measurement.

This modulation is very likely linked to the signal acquisition via the lock-in amplifier. In our setup, a reference frequency is supplied to the UHFLI (Zurich Instruments), which amplifies signals matching this reference. Consequently, if an external electromagnetic wave or mechanical vibration with a frequency close to the reference beat frequency is present, it may also be amplified and mixed into the measured signal. The resulting signal modulation is not constant but fluctuates slightly, which we attribute to the fact that the external modulation frequency does not exactly match the reference beat frequency. Notably, the reference frequency itself is continuously and automatically recalibrated to account for the minute fluctuations in the ASOPS lasers, which guarantees an acquisition at the same relative laser positions over multiple iterations This leads however to a central question: is the measured signal genuinely representative of the sample's response time or is it a result of external frequency components modulating the original ASOPS signal. To address this issue, we adjusted the delay frequency between the two pulses used in the measurement. This adjustment significantly reduced the temporal variations in the signal, leading to a more uniform and acquisition-time-invariant dataset, as shown in **Figure S6**.

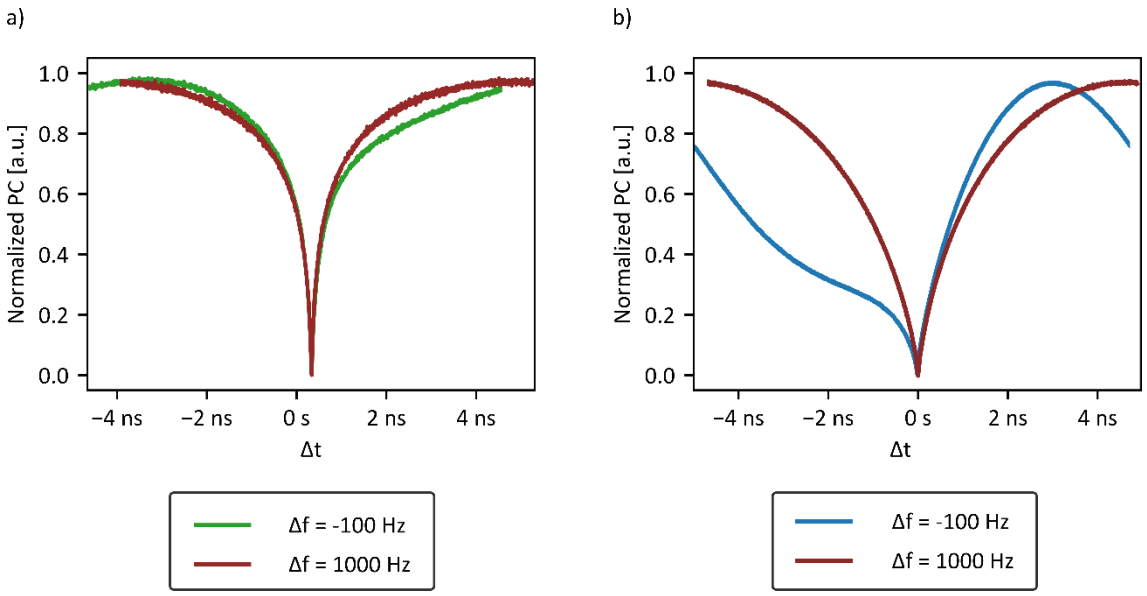

Figure S6: a) AOSPS data of PbS/EDA-exchanged nanoparticles acquired while nearby measurement instruments were operating, recorded with a delay frequency (Δf) of -100 Hz (Green) and 1 KHz (red). **b)** AOSPS data of the same sample with the cryostat actively operating. With measurements performed with Δf = -100 Hz (blue) and Δf = 1 KHz (red). The difference in starting and ending point of the datasets is due to the positioning of the Δt = 0, and how many datapoints are on either side. A negative beat frequency means that pump and probe lasers were switched, and the spectrum is therefore mirrored in relation to the Δf = 1000 Hz measurement.

Adjusting the beat frequency almost completely removed the signal modulation in our spectra. This results in highly symmetrical signals, as expected from the basic principles of ASOPS. However, the fact that such a change in beat frequency significantly alters the signal behaviour raises the question whether the measured signal is a true representation of the sample's intrinsic response time or if it is influenced (at least partially) by external frequency components modulating the original ASOPS signal. This concern is particularly relevant given the observation of a second, previously unreported fast decay component. To investigate this and verify the integrity of our measurements, we conducted a systematic study on the effect of varying the beat frequency on the acquired signal. Importantly, these measurements were performed independently of those shown in **Figure S6**, ensuring that no influence from the cryostat pump or other external instrumentation was present during acquisition. The purpose of this investigation was specifically to validate the presence of the fast component observed in our PbS/EDA samples and to determine whether changes in the beat frequency alter this signal in any significant way. The results of this study are presented in **Figure S7**, which compares two measurements obtained using different beat frequencies to assess their influence on the observed signal.

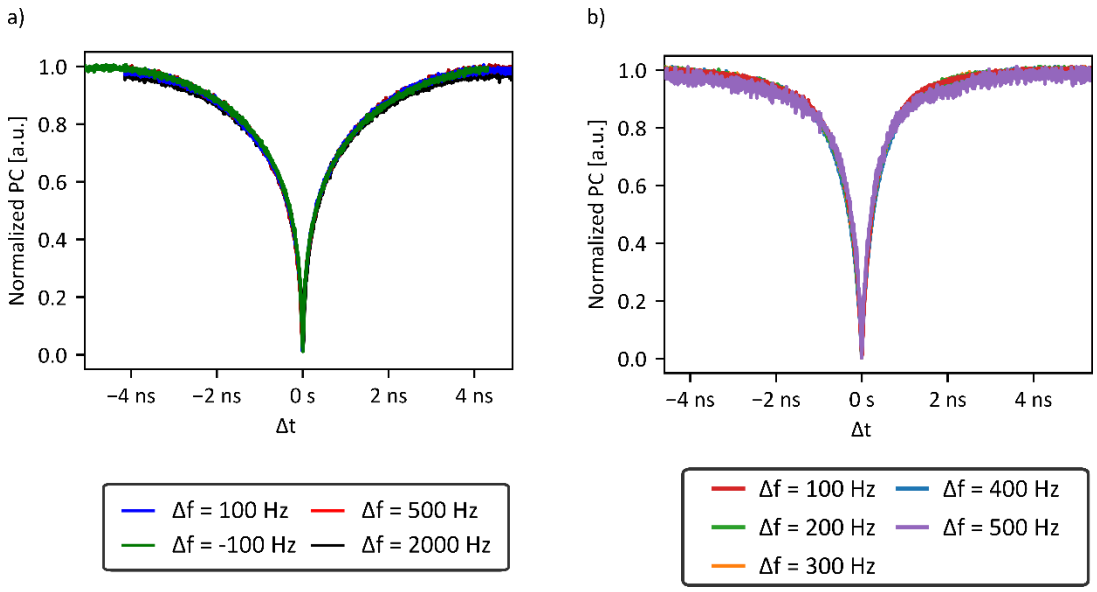

Figure S7: Measurements of PbS/EDA films under vacuum at various beat frequencies**. a)** and **b)** were measured at different days and with different batches of nanoparticles to attempt to verify the integrity of the measurements. The differences in response times are apparent when comparing a) and b).

As we can see in **Figure S7**, changing the beat frequency does not influence the received signal, leading us to conclude that the received signal is genuine and not a result of external influences. As previously mentioned, the measurement performed at Δf = -100 Hz is mirrored in relation to the Δf = 100 Hz measurement, however the fact that its shape coincides with the other spectra further highlights the symmetrical nature of our datasets. The remaining spectra with positive delay frequencies are also highly symmetrical, validating the present results. Further, several observations support the genuine nature of the signal. First, the signal's characteristics can be systematically tuned by varying the sample's temperature, pressure, and ligand shell. Since these are intrinsic sample parameters, their influence on the signal strongly suggests that the response arises from the sample itself. If the modulation were dependent on the influences of the surrounding instrumentation, such dependencies would not be expected. Additionally, the role of data averaging is important to consider. Each final dataset is the result of averaging between 10^5 and 10^7 individual samples. Even if a minor signal modulation were present, such averaging would either effectively suppress it or reveal its absence, particularly when no asymmetry is observable in the obtained data.

3.2. Material and ligand exchange characterization

To demonstrate consistency in the decay times between different synthesis batches, **Figure S8** presents a comparison of measurements obtained from two different PbS nanoparticle batches obtained with the same procedure.

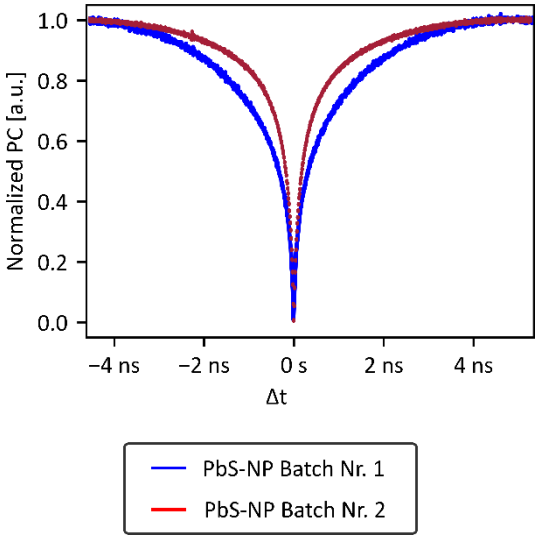

Figure S8: Measurements of different Batches of PbS nanoparticles, functionalized with EDA, under vacuum. The first batch (blue) was used for the presented results, while the second batch (red) serves as verification for the measured signal.

Both batches display comparable behaviour, thereby confirming the reproducibility of the results and reducing the likelihood that the measured response times originate from specific synthetic conditions (such as impurity doping). While absolute decay time speeds differ between the exemplary datasets (Batch 1: .1.3 ns / 130 ps, Batch 2: 1.1 ns / 130 ps), these values should only be discussed within an order of magnitude (eg ≈1ns/≈100 ps) , as previously noted. A more extensive statistical analysis would be required to rigorously evaluate potential variations in response speed. However, we surmise that there is no difference in the nanoparticles behaviour as far as our measurements are concerned as the underlying mechanisms necessitating a two-component fit are consistently observed in both measurements and the decay times are well within the statistical analysis in Section 6 of this SI.

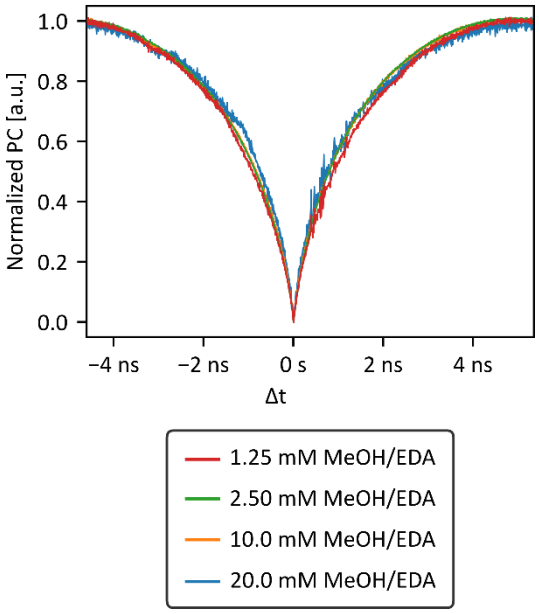

Figure S9: Measurements of PbS/EDA nanoparticles under vacuum, prepared with EDA/MeOH solutions with different EDA concentrations.

In **Figure S9**, the influence of ligand concentration during the exchange process is presented. No clear trend is discernible within the analysed concentration range.

3.3. Additional oxygen and nitrogen gas characterization

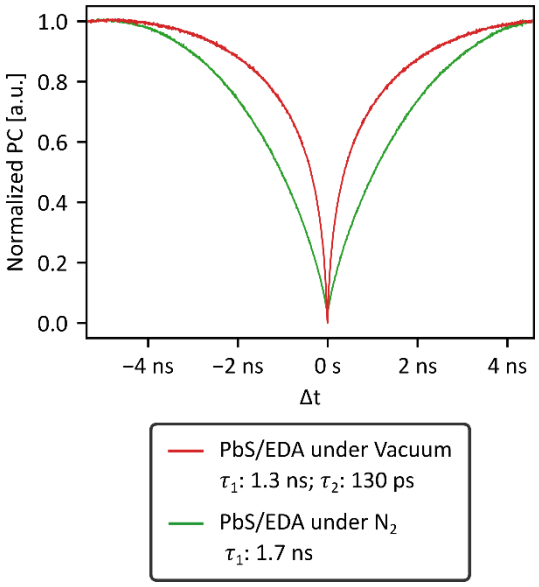

Figure S10: Comparison of PbS/EDA under vacuum (red) and upon reintroduction of N_2 gas (green).

In **Figure S10** the nanoparticle response times are compared under vacuum (red) and after refilling the chamber with N_2 (green). Under N_2, the response can again be described by a single decay component, indicating that the process is reversible. Looking at the influence of atmospheric conditions, especially in contrast to the behaviour under vacuum, we can see that the measured photocurrent decreases over time, while measurements over the same timeframe under vacuum show no such degradation. This is shown in **Figure S11**.

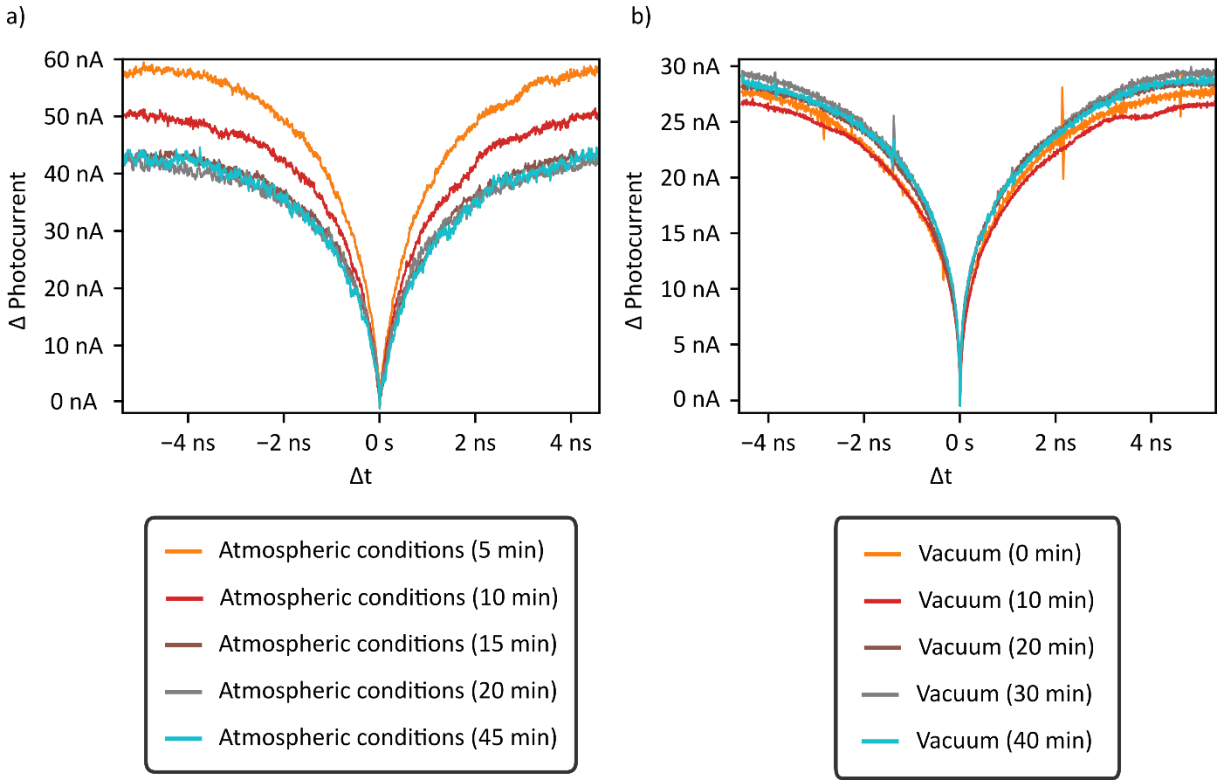

Figure S11: a) Non-normalized comparison of PbS/EDA nanoparticles over time under ambient conditions. b) Non-normalized measurements of PbS/EDA nanoparticles recorded over a comparable timescale time under vacuum.

It should be noted that the measurements presented in **Figure S11** were not performed on the same day. Consequently, the photocurrent values should only be considered for internal comparison within each dataset and not across different samples, as absolute values may vary between measurements. A direct comparison of photocurrent obtained under vacuum and after subsequent exposure to atmospheric conditions is provided in **Figure S12 a)**. **Figure S12 b)** shows a normalized image of the results shown in **Figure S11 a)** to show that the mechanistic decay processes remain constant despite the reduction in photocurrent.

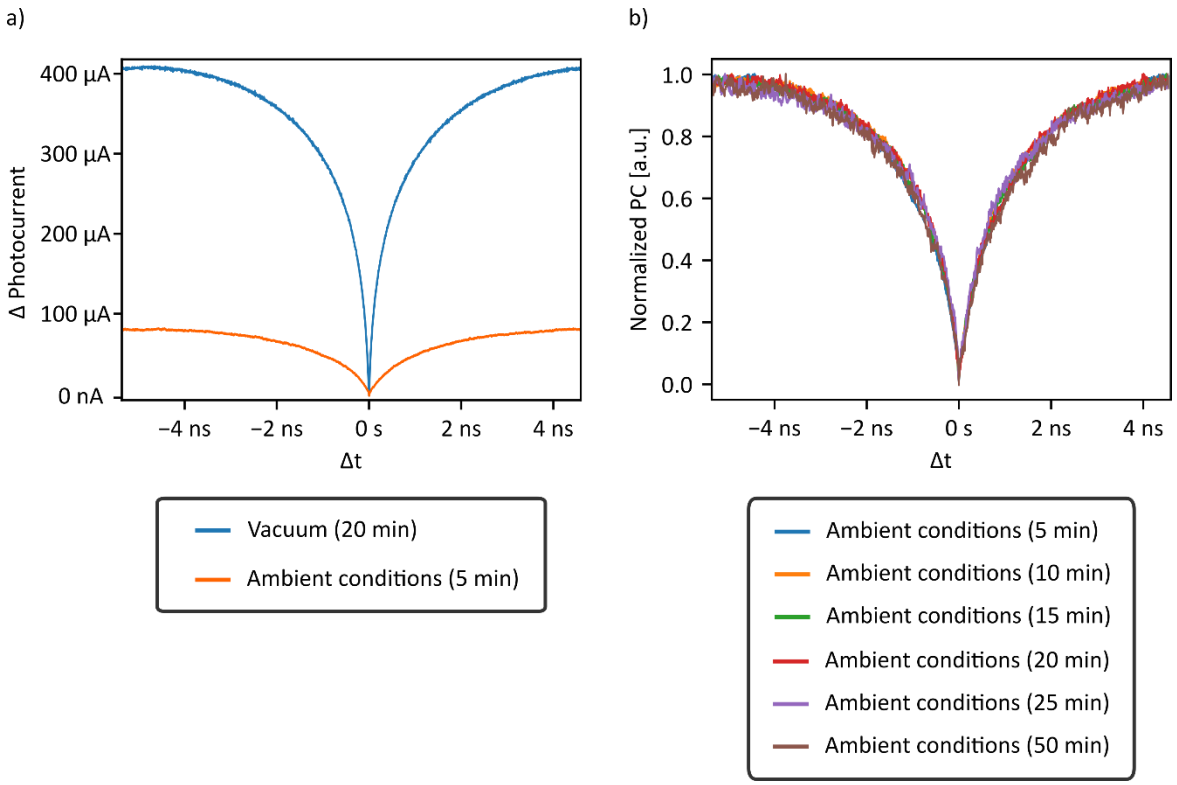

Figure S12: Comparison of the same PbS/EDA sample measured under vacuum after 20 minutes (blue) and after exposure to ambient conditions after 5 minutes (orange).

3.4. Ultrafast component

Finally, we briefly address the ultrafast signal discussed in the main text and presented in **Figure S13.**

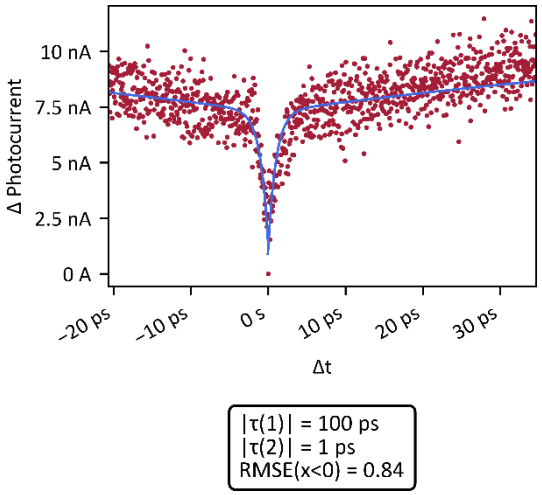

Figure S13: Measurement of a ultrafast PbS signal as well as the corresponding fit

Based on the preceding analysis of signal modulation, we conclude that this component is indeed genuine, although its amplitude is relatively small in comparison to the overall photoresponse. For context, the typical photocurrent observed within our 10 ns measurement window is approximately 100 nA at 5V. The presence of a slight asymmetry, however small, hinders the stating of absolute timing values to this feature, however, despite this limitation, we consider the observed timescale of approximately 1 picosecond to be rather accurate, based on an observation of the data with its corresponding fit. Its absence from the data presented in the main text and SI is attributed to the limited temporal resolution of the UHFLI system, which acquires 1024 data points per spectrum. Given a total time window of 10 ns, this corresponds to a temporal resolution of approximately 9 ps and is therefore insufficient to resolve features on the 1 ps timescale. Although this signal may be of interest for future investigations, particularly due to its ultrafast dynamics, it was not examined in greater detail as it does not significantly influence the overall photoresponse due to its small magnitude.

4. Random Sampling with Replacement

To verify the robustness of the fits and the validity of the observed signals, we employ a bootstrapping method, using random sampling with replacement. In this method, random data pairs are selected from the original dataset to generate new, synthetic datasets. Each of these datasets is then automatically fitted using initial parameters derived from the preliminary fitting. In **Figure S14 a)**, the original dataset is plotted and fitted (via MATLAB), where the starting parameters for both response times are manually estimated. The algorithm subsequently determines the best-fit parameters by minimizing the fitting error. The model used for the two-component case follows the previously described equation:

$$y(\Delta t) = A * e^{-\frac{\Delta t}{\tau(1)}} + B * e^{-\frac{\Delta t}{\tau(2)}} + c \qquad 1$$

Here, A and B represent the amplitudes corresponding to the decay times $\tau(1)$ and $\tau(2)$, respectively. The variable Δt denotes the delay time and c is the offset along the y-axis. The parameters obtained from the initial fit are then used as the starting values for fitting each of the 1000 bootstrapped datasets. This allows for a statistical evaluation of the variability and stability of the fitting parameters. The resulting distributions of decay times are presented in **Figures S14 b)** and **S14 c)**. To assess the reliability of the fitted response times, we analyse the distribution of data points by plotting the amplitudes A and B against their corresponding decay times, as shown in **Figures S14 d) and S14 e).** Although these plots can provide more detailed insights, for our purposes it is sufficient to evaluate whether the parameters are correlated. The observed correlations suggest that the fit is generally robust. However, special caution must be taken in interpreting the parameter $\tau(2)$, as subtle trends may be overlooked and attributed to minor fitting variations. These variations, while potentially meaningful within the observed time regime, do not result in a sufficiently significant change in fit quality to draw definitive conclusions. Therefore, in the main manuscript, we focus primarily on the amplitudes A and B, and their mutual correlation, to evaluate changes in the system.

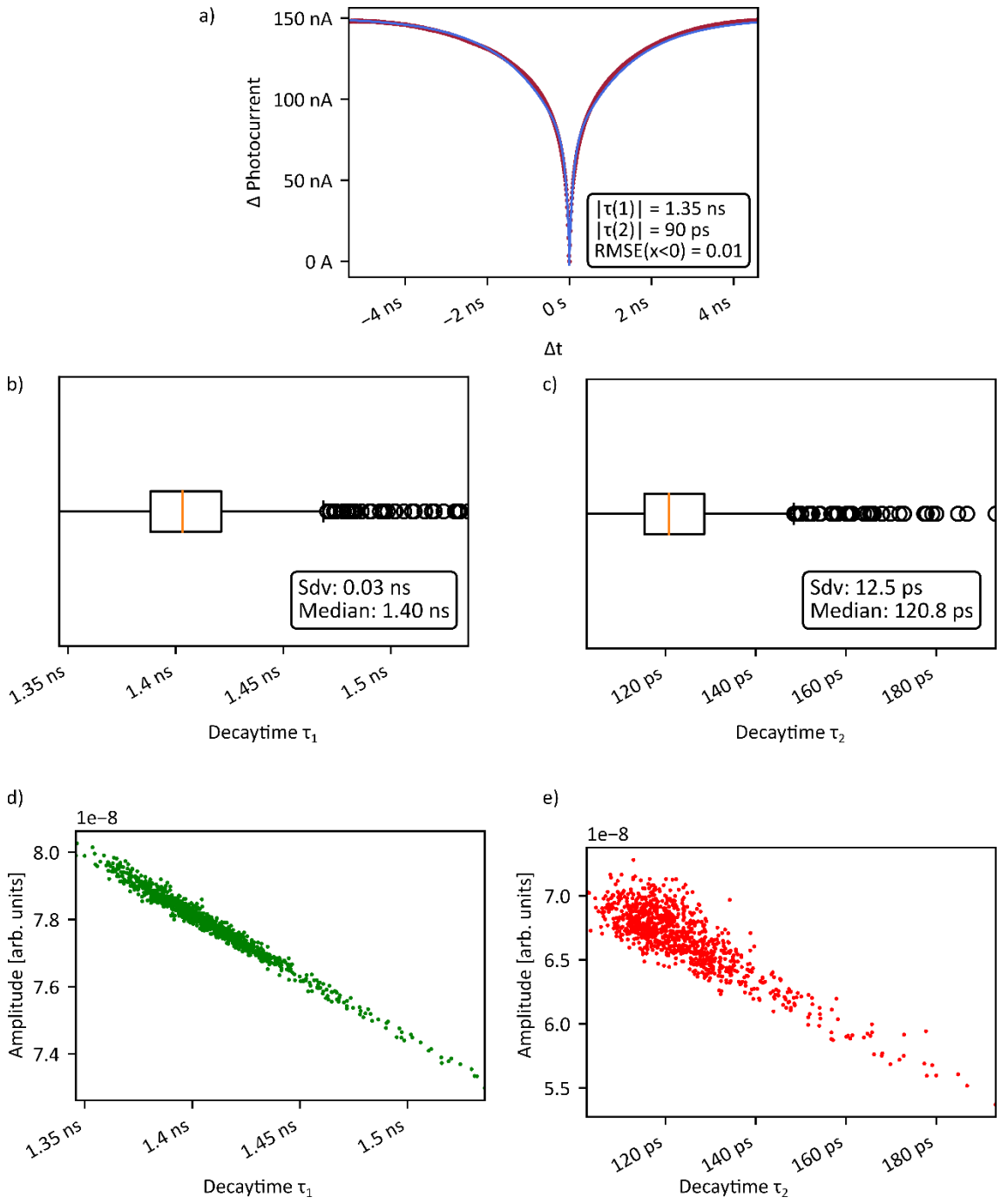

Figure S14: a) Initial fit of a PbS/EDA measurement. The fit was only performed for the data Δt < 0 and then mirrored onto the right side of the spectrum. **b,c)** boxplots of the received values for $\tau(1)$ and $\tau(2)$ after random sampling with replacement. **d,e)** Amplitudes A and B plotted against $\tau(1)$ and $\tau(2)$ respectively.

5. Temperature dependent parameter correlation

Since the absolute values of the response times are not sufficiently specific to capture the relative changes of the individual decay processes as a function of temperature, we employ the ratio $\frac{B}{A+B} * 100$, as a simplified metric to estimate the contribution of the second decay component to the overall signal (B_{rel}). In this context, A and B represent the amplitudes of the first and second decay components, respectively, as defined in Equation (1). This approach is applied to the dataset presented in the main manuscript, yielding the values summarized in the following table.

Table 1: Overview of the data from the temperature dependent measurements after Random sampling with replacement.

T [K]	A	B	$\frac{B}{A+B} * 100$ [%]	$\tau(1)$ [ns]	$\tau(2)$ [ps]
300	$4.00 * 10^{-8}$	$2.95 * 10^{-8}$	42.5	1.39	138
280	$9.98 * 10^{-8}$	$2.08 * 10^{-8}$	17.3	1.53	214
250	$1.32 * 10^{-7}$	$1.88 * 10^{-8}$	12.5	1.65	200
200	$7.73 * 10^{-8}$	$8.00 * 10^{-7}$	9.4	1.77	173

As shown in the table, the absolute values of the response times of τ(2) do not exhibit a consistent trend. In contrast, the amplitudes of the decay components vary significantly, highlighting a decrease in the contribution of this second (picosecond) component. This is also evident in **Figure 3** of the main manuscript, where the change in the spectra can be followed as a function of temperature. Consequently, we use the amplitude ratio as a metric to characterize the behaviour of the system.

6. Quantitative analysis

Despite the variance in the extracted response times which limits the reliability of statements regarding absolute timescales, we aim to provide an overview of multiple measurements to demonstrate both the reproducibility of the results, and the general range of timescales observed. **Figure S15** presents such an overview, displaying data from 43 individual measurements conducted under consistent conditions: room temperature (290–300 K), pressure approximately 1×10^{-5} mbar, and a beat frequency of Δf=−100.

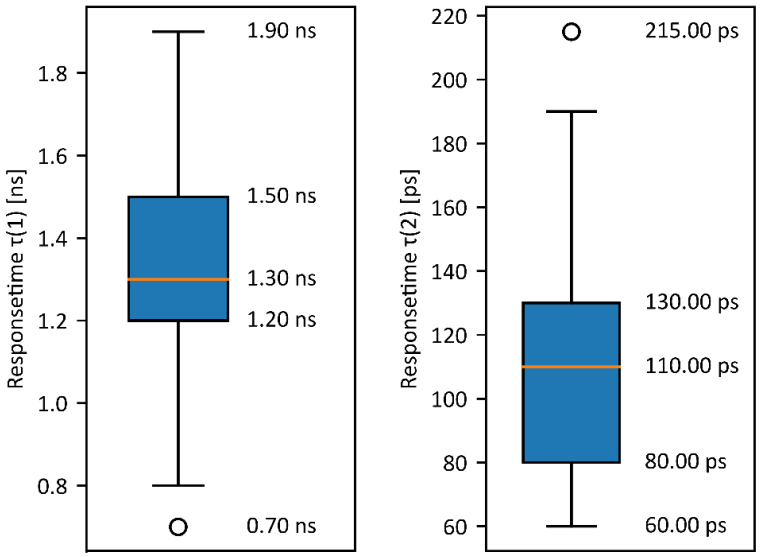

Figure S15: Boxplot of the slow components τ(1) (left) and fast components τ(2) (right) of 43 individual measurements. All values present results from the first performed fit on the data (not the succesive bootstraping analysis), and were aquired under the same experimental conditions: room temperature (290–300 K), pressure approximately 1×10^{-5} mbar, and a beat frequency of Δf=−100

7. Extrinsic Measurements

To contextualize the intrinsic measurements within the broader scope of the electric properties, I/U curves of both PbS-QD species are measured in the absence of illumination. Although substantial variations in several orders of magnitude occurred from film to film for both types, only samples with sheet resistances in the order of $10^{11}\Omega/sq$ to $10^{12}\Omega/sq$ were used for further investigation (**Figure S16 a**). Deviations below or above this range were interpreted as indicating insufficient film quality or short-circuiting. Sheet resistance was chosen as a comparable unit because no information about film thickness could be acquired due to the film's oxygen sensitivity and subsequent decay.

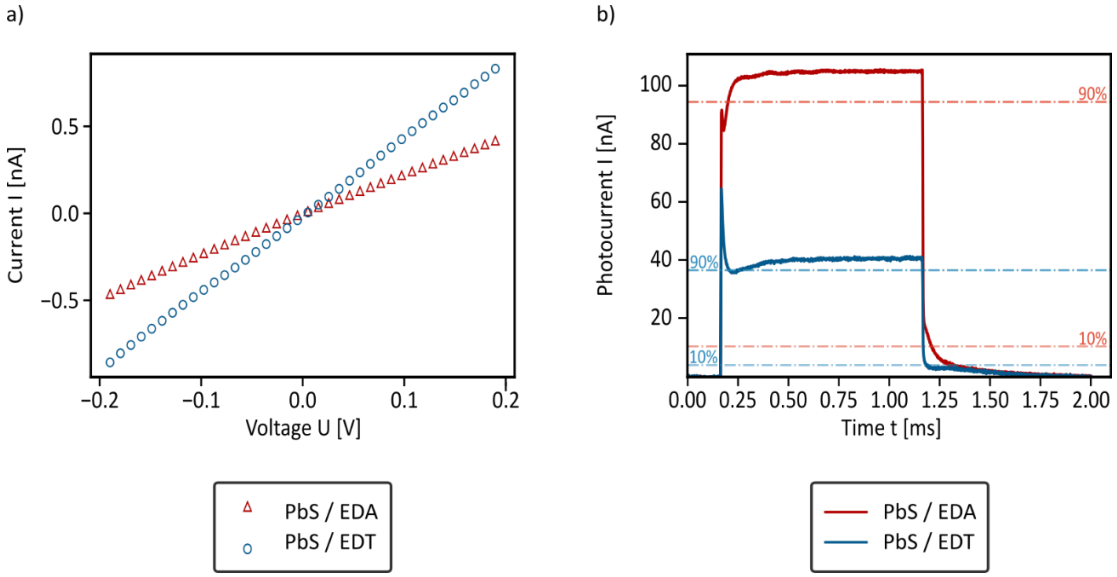

Figure S16 a) I /U curves without illumination reveal conductivities for EDA (red) $\sigma = 2.89 \cdot 10^{-5} S(m^{-1})$ and EDT (blue) $\sigma = 5.54 \cdot 10^{-5} S(m^{-1})$ functionalized PbS-QD thin films with an approximated film thickness of 20 nm. **b)** square pulse measurement of EDA (red) and EDT (blue) functionalized PbS-QD thin films at 300 K under 3 V bias voltage with a 635 nm laser and a set frequency of 500 Hz. Dotted lines highlight 10 % and 90 % levels of the photocurrent to quantify respective rise and fall times. While EDA exhibits higher photocurrents, the rise ($\tau_{rise} = 36\ \mu s$) and fall times ($\tau_{fall} = 45\ \mu s$) are slower than respective values from EDT ($\tau_{rise} = 3\ \mu s;\ \tau_{fall} = 19\ \mu s$).

Figure S16 b) shows extrinsic photo response measurements of functionalized PbS-QD thin films, conducted at 300 K under an applied bias of 3 V and continuous-wave (CW) laser illumination (λ = 635 nm, power = 1.9 mW, with ~99.75% optical loss due to fiber coupling). While EDA functionalized particles yielded photocurrents on the order of 10^{-7} A, EDT-functionalized systems under identical conditions exhibit photocurrents that are approximately half of this value. Nevertheless, deviations within individual samples of both types vary down to a few hundred pico amperes and are attributed to different film qualities and thicknesses. It could be shown that EDT-liganded PbS-QDs exhibit faster response times ($\tau_{rise} \sim 10^{-6}$ s; $\tau_{fall} \sim 10^{-5}\ s$) in comparison to EDA covered ones ($\tau_{rise} \sim 10^{-5}$ s; $\tau_{fall} \sim 10^{-5}\ s$). Both systems seem to be rather fast compared to other reported PbS photodetectors[2]. Nonetheless, it is important to note that variations in response times are again attributable to film inhomogeneities and could be measured between different samples as well as for individual channels. In particular, the slow components, which are closely related to the film quality and interband trap states, may be the reason for varying results between individual measurements[3,4].

These extrinsic measurements do not demonstrate significant disparity between N_2 atmosphere or vacuum conditions, nor do they exhibit a significant tendency to distinguishable decay components as observed for the intrinsic measurements. Consequently, this effect is not observed in temperature-dependent measurements either. The absence of the same dependency as reported for intrinsic measurements within this work is most likely a result of one of the following arguments or an interplay of these: First, the decay timescales differ significantly between intrinsic and extrinsic measurements and thus, are not measurable extrinsically. Furthermore, different limiting factors that contribute to

extrinsic measurements (e. g. RC-time, transit-time) prevent similar decay times for both types of measurement. Additionally, the presence of slow components, induced by e. g. trap states, can overlap with faster components and impede quantification.[5] The photocurrent itself is found to decrease in accordance with decreasing temperature which is also in agreement with S. Pichler et al[6].

8. Literature

(1) Urich, A.; Unterrainer, K.; Mueller, T. Intrinsic Response Time of Graphene Photodetectors. *Nano Lett.* **2011**, *11* (7), 2804–2808. https://doi.org/10.1021/nl2011388.

(2) Schedel, C.; Strauß, F.; Scheele, M. Pitfalls in Determining the Electrical Bandwidth of Nonideal Nanomaterials for Photodetection. *J. Phys. Chem. C* **2022**, *126* (32), 14011–14016. https://doi.org/10.1021/acs.jpcc.2c04584.

(3) Pichler, S.; Rauch, T.; Seyrkammer, R.; Böberl, M.; Tedde, S. F.; Fürst, J.; Kovalenko, M. V.; Lemmer, U.; Hayden, O.; Heiss, W. Temperature Dependent Photoresponse from Colloidal PbS Quantum Dot Sensitized Inorganic/Organic Hybrid Photodiodes. *Applied Physics Letters* **2011**, *98* (5), 053304. https://doi.org/10.1063/1.3552678.

(4) Huang, W.; Wang, S.; Gong, H.; Tian, J.; Peng, J.; Cao, J. Size Tunable and Controllable Synthesis of PbS Quantum Dots for Broadband Photoelectric Response. *Optical Materials* **2023**, *142*, 113977. https://doi.org/10.1016/j.optmat.2023.113977.

(5) Strauß, F.; Zeng, Z.; Braun, K.; Scheele, M. Toward Gigahertz Photodetection with Transition Metal Dichalcogenides. *Acc. Chem. Res.* **2024**, *57* (10), 1488–1499. https://doi.org/10.1021/acs.accounts.4c00088.

(6) Pichler, S.; Rauch, T.; Seyrkammer, R.; Böberl, M.; Tedde, S. F.; Fürst, J.; Kovalenko, M. V.; Lemmer, U.; Hayden, O.; Heiss, W. Temperature Dependent Photoresponse from Colloidal PbS Quantum Dot Sensitized Inorganic/Organic Hybrid Photodiodes. *Applied Physics Letters* **2011**, *98* (5), 053304. https://doi.org/10.1063/1.3552678.